Numerical Analysis and Validation of a Pressure-Differential Wave Energy Converter

Fabian Wendt*, Yi-Hsiang Yu*, Aurélien Babarit†, Mike Delos-Reyes‡

*National Renewable Energy Laboratory (NREL)
Golden, Colorado 80401, USA
E-mail: fabian.wendt@nrel.gov, yi-hsiang.yu@nrel.gov
†EC Nantes, LHEEA Lab.
Nantes, France
E-mail: aurelien.babarit@ec-nantes.fr
‡M3 WAVE
Corvallis, OR, USA
E-mail: info@m3wave.com

***Abstract*—A pressure-differential wave energy converter (WEC) is a unique design, compared to conventional kinematic WECs. It contains two flexible, air-filled bags that turn pressure fluctuations caused by ocean waves and swells into alternating expansion and compression cycles. The two bags are strategically oriented based on the dominant wave environment and exchange air back and forth with each passing wave. A turbine is located between the two bags and used to extract power from the internal airflow.**

A fixed-bottom pressure-differential design can be directly analyzed in the frequency domain by modeling the bag motion as a generalized body mode. However, for a floating system, the device motion influences its power output and a coupled analysis approach is required. As a result, the authors developed a time-domain numerical model to analyze the floating pressure-differential WEC system.

The equations of motion describing the bag and rigid body motion of the device are solved in a coupled fashion. The hydrodynamic diffraction and radiation coefficients for all relevant system motions have been computed via WAMIT. The bag motion was introduced within WAMIT as an additional generalized body mode. The hydrodynamic performance of the system is validated against 1:50-scale wave tank measurements and the influence of motion coupling on the power performance is characterized.

***Index Terms*—wave energy, pressure differential, generalized modes, WAMIT, M3**

I. Introduction

Numerous studies have shown that extracting energy from ocean wave resources has the potential to provide a significant contribution to the electricity supply [1]. In the past several decades, a wide variety of wave energy converter (WEC) technologies has been proposed, including oscillating water columns, oscillating body type designs, and over-topping devices [2]. However, wave energy technology is still in the research and development stage. Therefore, levelized cost of energy (LCOE) for WEC designs is still high, compared to other renewable energy technologies, such as wind and solar [3].

Although the cost may gradually decrease with industrialization and mass production as large WEC farms are being developed, it is essential to find an efficient pathway to reduce that cost for the WEC industry to be successful. Several innovative WEC technologies have been proposed recently, including the use of flexible material that will minimize the load on the device and reduce the overall LCOE [4]–[6]. This work is focused on pressure-differential wave energy conversion, which is a unique approach compared to conventional kinematic WECs. Pressure-differential WECs contain two (or more) air-filled bags that turn ocean-wave-induced pressure fluctuations into alternating expansion and compression cycles, as shown in Fig. 1. The two bags are strategically oriented based on the dominant wave environment and exchange air back and forth with each passing wave. A study on a bottom-fixed pressure-differential WEC was conducted by Babarit et al. [4], which indicated that the pressure-differential WEC could be highly efficient both with respect to energy absorption and economic potential.

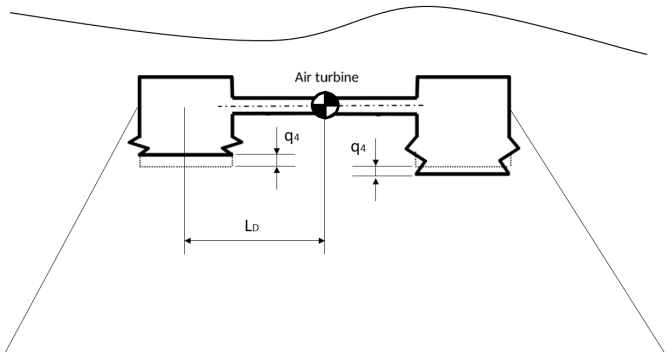

Fig. 1. A taut moored M3 device with a piston-type bag mode shape. Graphic based on [4].

II. Numerical Model

A numerical model was developed to simulate the taut moored M3 device for regular wave conditions. M3 Wave LLC is a company out of Oregon that has been developing the

pressure-differential wave energy technology since the early 1990s [7].

In this work, the numerical model was solved in the time domain to account for quadratic damping components. The convolution integral that is typically used in Cummins-type time domain models [8] was not implemented, because of the fact that only regular wave cases were investigated and no significant nonlinear behaviour of the model was to be expected. The bag displacement is modeled as a piston type motion (Fig. 1). The utilized equations of motion are based on the work presented in [4], but additional degrees of freedom have been introduced to account for the motion of the device in its moored configuration. Compared to [4], an additional constraint has been formulated by modeling the bag motion as a single mode shape (e.g., the left bag moves down and the right bag moves up). This additional constraint was introduced to further simplify the equations of motion. Due to the fact that only one wave direction was considered here, only the surge (1), heave (2), pitch (3), and bag motion (4) degrees of freedom were included in the numerical model. The equations of motion used in the numerical model are outlined below. They are formulated at the center of gavity which is located at the geometric center of the device (see Fig 1).

$$\mathbf{A}\ddot{\mathbf{q}} + \mathbf{B}\dot{\mathbf{q}} + \mathbf{D}\mathbf{v} + 0.5\mathbf{S}(\mathbf{p_1} + \mathbf{p_2}) + (\mathbf{K} + \mathbf{C})\mathbf{q} = \mathbf{F_{ex}} \quad (1)$$

$$\dot{p_1} - 0.5\frac{p_s}{v_s}\mathbf{R}\dot{\mathbf{q}} + \frac{p_s}{v_s}\frac{p_1}{B_{PTO}} - \frac{p_s}{v_s}\frac{p_2}{B_{PTO}} = 0 \quad (2)$$

$$\dot{p_2} + 0.5\frac{p_s}{v_s}\mathbf{R}\dot{\mathbf{q}} - \frac{p_s}{v_s}\frac{p_1}{B_{PTO}} + \frac{p_s}{v_s}\frac{p_2}{B_{PTO}} = 0 \quad (3)$$

The matrix $\mathbf{S}$ is only populated along the main diagonal and describes the relevant surface area that is participating in the coupled motion response between the rigid body modes and bag motion (Eq. 4):

$$\mathbf{S}_{ii} = \int\int_{A_4} m_4 w_i dS \quad i = \{1..4\} \quad (4)$$

$$m_j = \mathbf{M_j}(\mathbf{x}) \cdot \mathbf{n_g} \quad j = \{1..4\} \quad (5)$$

$$\mathbf{C}_{ij} = d_{ij} \int\int_{A_j} m_j w_i dS \quad i, j = \{1..4\} \quad (6)$$

$$d_{ij} = \rho g \quad \forall\{i < 4 \wedge j < 4\} \quad (7)$$

$$d_{ij} = (\rho - \rho\prime)g \quad \forall\{i > 3 \vee j > 3\} \quad (8)$$

With m_j being the normal component of the jth mode shape relative to the body surface and w_i being the vertical component of the displacement vector of the ith mode.

The scalar value, m_j, is being computed as the dot product of the local mode shape displacement vector, $\mathbf{M_j}(\mathbf{x})$, at the location $\mathbf{x}$ on the body surface, and the normal vector, $\mathbf{n_g}$, that points from the wetted surface participating in the jth mode shape, (A_j), into the body. The 4x1 vector, $\mathbf{q}$, and its derivatives describe the motion of the system (displacement, velocity, and acceleration) of the four degrees of freedom present in the system (three rigid body modes and one generalized mode).

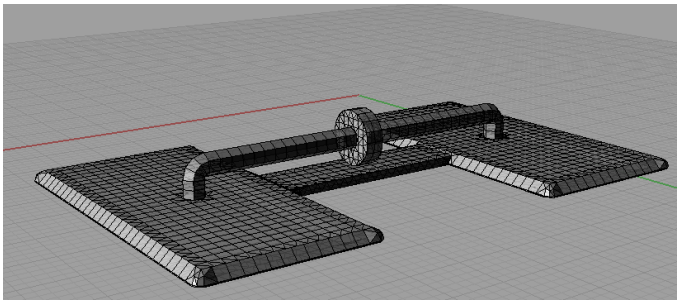

Fig. 2. Top isometric view of the WAMIT mesh.

The 1x4 row vector, $\mathbf{R}$, contains the same entries as the diagonal of the $\mathbf{S}$ matrix, arranged in a single row, and describes how the bag deforms as a result of coupled motion.

The $\mathbf{p_1}$ and $\mathbf{p_2}$ vectors are simply populated with the p_1 and p_2 values: $\mathbf{p_{1_i}} = p_1$ and $\mathbf{p_{2_i}} = p_2$ for $i = 1$ to 4.

The $\mathbf{A}$ matrix contains mass and inertia contributions from the device itself and from added mass effects. $\mathbf{B}$ is the linear radiation damping matrix. Frequency-dependent added mass and radiation damping are computed via WAMIT.

The $\mathbf{K}$ matrix represents the linear restoring contribution from the mooring system and the $\mathbf{C}$ matrix contains the hydrostatic stiffness terms as described in Eq. 6.

Quadratic damping resulting from viscous effects is included in the equation of motion through the $\mathbf{D}$ matrix and the $\mathbf{v}$ vector as outlined in Eq. 9 and Eq. 10. A value of 8.0 was assigned to the viscous drag coefficient, C_d. Drag coefficients in the range between 8 and 10 are oftentimes used to model viscous effects in heave plates for offshore structures [9], [10].

$$\mathbf{D} = \begin{bmatrix} 0 & 0 & 0 & 0 \\ 0 & \mathbf{S}_{4,4}C_d & 0 & 0 \\ 0 & 0 & \frac{1}{2L_D}\mathbf{S}_{3,3}C_d & \frac{1}{2L_D}\mathbf{S}_{3,4}C_d \\ 0 & 0 & \frac{1}{2L_D}\mathbf{S}_{3,4}C_d & \mathbf{S}_{4,4}C_d \end{bmatrix} \quad (9)$$

$$\mathbf{v} = \begin{bmatrix} \dot{\mathbf{q}}_1^2 \\ \dot{\mathbf{q}}_2^2 \\ (\dot{\mathbf{q}}_3 L_D)^2 \\ \dot{\mathbf{q}}_4^2 \end{bmatrix} \quad (10)$$

The water density, (1025 $\frac{kg}{m^3}$), is given as ρ, while $\rho\prime$ describes the density of the working fluid inside the wave energy device (in this case, air with 1.225 $\frac{kg}{m^3}$). The equations of motion (Eq. 1–Eq. 3) can be formulated as a system of differential equations and solved numerically. The linear damping, added mass, and wave-excitation loads ($\mathbf{F}_{ex}$) caused by Froude-Krylov and scattering forces were computed via WAMIT [11]. An illustration of the utilized WAMIT mesh is shown in Fig. 2 and Fig. 3. The bag area that is participating in the piston motion is highlighted in orange.

III. Wave Tank Testing

A 1:50-scale version of the taut moored M3 device has been tested in the tow tank of the Marine Hydrodynamics

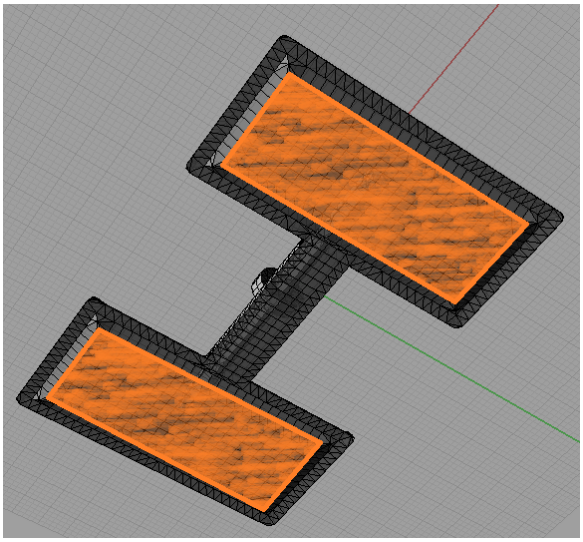

Fig. 3. Bottom isometric view of the WAMIT mesh; the bag surface participating in the piston mode shape is highlighted in orange.

Fig. 4. Marine Hydrodynamics Laboratory tow tank and carriage [12].

Laboratory at the University of Michigan during the U.S. Department of Energy Wave Energy Prize in January 2016 [12]. The goal of the tests was the experimental characterization of the system's power performance over a range of different wave conditions. The M3 device uses a turbine in the middle of the tube that connects the two flexible chambers to generate electrical power. For the model-scale test, the turbine was modeled through a simple orifice plate. The plate geometry was selected so that it produces a pressure drop similar to what would be expected from a model-scale turbine. Photos of the tow tank and the M3 device installed in the tow tank are shown in Fig. 4 and Fig. 5, respectively.

During the test, the generated power was computed from the measured pressure drop over the orifice plate. The exact procedure that was used to transfer the pressure measurements into an estimate of the generated power was not available to the authors. The device motions were recorded through an optical measurement system. The exact position relative to the device center that was used to report these motions was not known

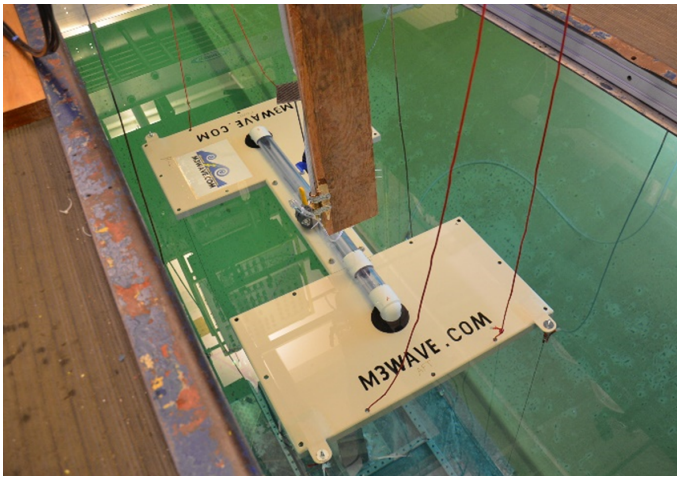

Fig. 5. Scaled M3 device installed in the tow tank [12].

to the authors. Because of the large uncertainties associated with the recorded time series data, the authors focused their validation efforts on the motion amplitude and average power production data that were reported in table format for each test case.

IV. Comparison of Fixed versus Floating System

To characterize the dynamic response of the numerical model, we computed the response amplitude operators (RAOs) and the averaged power production over a large range of different regular wave periods. Comparing a fixed versus a moored/floating configuration was one important aspect of our analysis. In the numerical model, the fixed configuration was realized by removing all coupling terms from the equations of motion (Eq. 1–Eq. 3). This approach yields a system of equations in which each degree of freedom is solved independently and the power performance and bag motion will not be impacted by the motion of the device (which basically represents a fixed system). Comparing the coupled and uncoupled numerical model makes it possible to quantify the impact of the device motion on the power performance of the system. All results presented and discussed in this paper are refering to the full scale version of the system. The length from chamber to device center (L_D in Fig. 1) for the full scale system is 25.0 m. The bottom of the device is submerged 12 m below the free surface.

Fig. 6 shows the pitch RAO of the numerical model with and without coupling terms. For the uncoupled model, we are only interested in the bag motion and power performance, as this configuration represents our fixed system and the pitch response of the uncoupled model is of little value in this analysis. A relatively large pitch response is evident for the coupled model for wave frequencies below 1 rad/s. When comparing the bag RAO (describing the piston-type bag surface displacement as illustrated in Fig. 1), a large bag response is evident for the coupled system below 1 rad/s (Fig. 7). However, this large low-frequency bag response

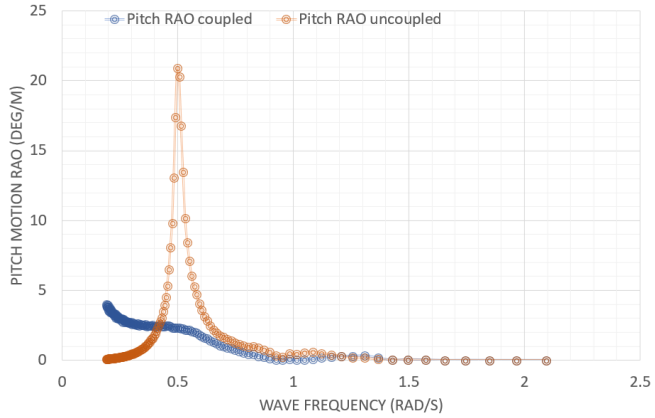

Fig. 6. Coupled/floating and uncoupled/fixed pitch motion response amplitude operator (RAO).

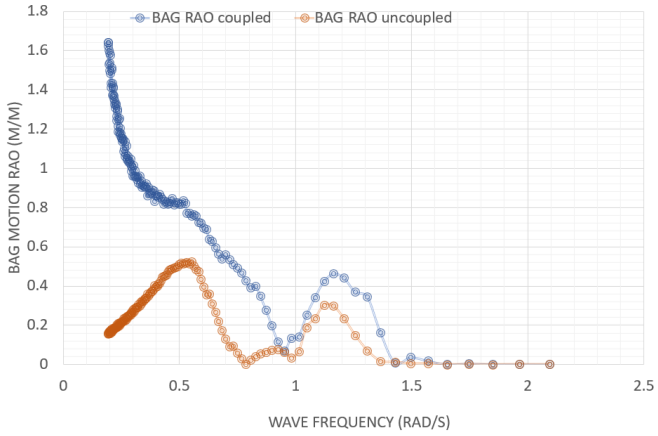

Fig. 7. Coupled/floating and uncoupled/fixed bag motion RAO.

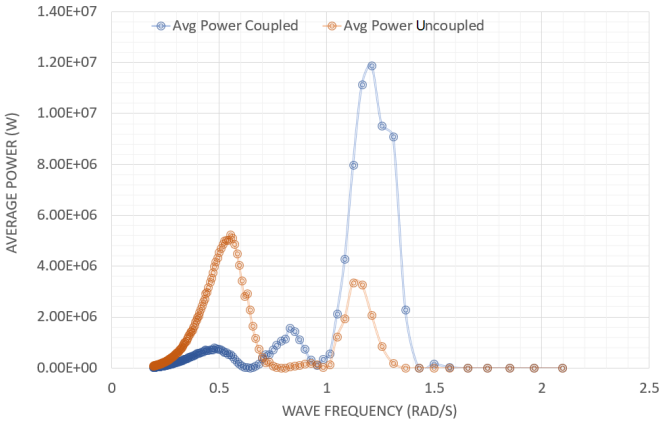

Fig. 8. Average power for coupled/floating and uncoupled/fixed system.

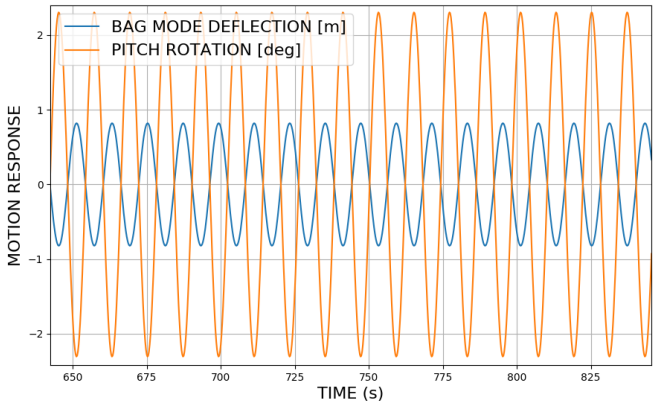

Fig. 9. Bag displacement and pitch motion time series during a 12-s regular wave.

does not result in a large average power output. For lower frequencies, the coupled system produces significantly less power than the uncoupled/fixed system (Fig. 8). The reduced power production of the coupled system for lower frequencies points to the fact that the relatively large pitch motion for lower frequencies has a negative impact on the power performance of the device.

The bag deflection and pitch motion time series plots for the 12-s wave period (0.52 rad/s) further illustrate the effect of coupling on the power production (Fig. 9). The pitch motion of the system and the bag deflection are almost perfectly out of phase.

This situation is shown in **Case B** of Fig. 10: the device experiences a positive pitch motion. The right chamber moves down and the right lower bag surface moves up. In this situation, the coupling between the bag and pitch motion reduces the pressure fluctuations in the chambers. The pitch motion by itself increases the hydrostatic and hydrodynamic pressure on the right bag surface, whereas the bag deflection counteracts this effect by moving air from the right chamber into the left chamber.

The opposite scenario can be observed for a wave period of around 5 s (**Case A** in Fig. 10). The bag and pitch motions are in phase and increase the pressure fluctuations in the chambers. The corresponding bag deflection and pitch motion time series are shown in Fig. 11. A wave period of 5 s is equivalent to about 1.26 rad/s, where a peak in average power can be observed for the coupled model in Fig. 8. For both **Case A** and **Case B**, the bag motion is dominated by wave-excitation forces, while the pitch motion amplifies or decreases the pressure fluctuations in the two bags, depending on the relative phasing between the pitch and bag motion.

For the current design, the coupling only has a positive impact on power performance for wave frequencies above 1 rad/s. For these higher frequencies, the waves are smaller in amplitude and carry less energy; therefore, taking advantage of this coupling effect is difficult.

V. Comparison against Experimental Data

The validation of the numerical model is not a straightforward process, because of the relatively large uncertainty associated with the experimental data. No detailed information on the mooring system properties were available to the authors. The mooring system was represented through a linear stiffness

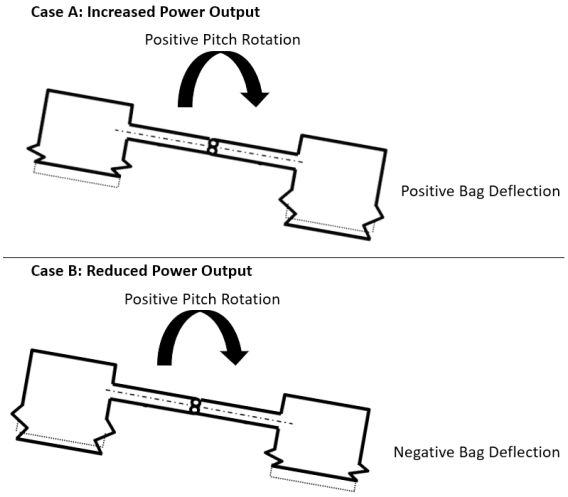

Fig. 10. Illustration of different bag/pitch coupling modi. The dotted lines represent the bag position in equilibrium when the device is leveled.

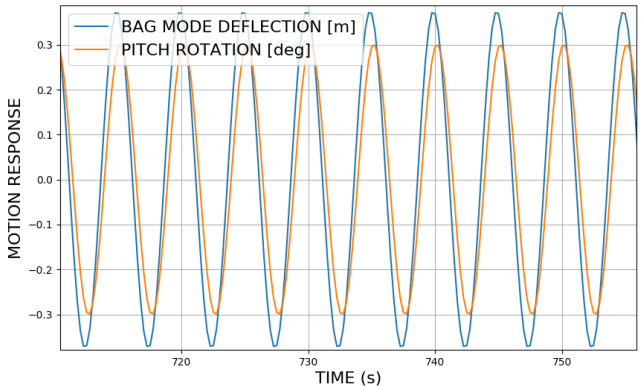

Fig. 11. Bag displacement and pitch motion time series during a 5-s regular wave.

TABLE I
REGULAR WAVE CASES USED FOR VALIDATION

ID	Period $[s]$	Freq. $[rad/s]$	Height $[m]$	B_{PTO} $[\frac{Ns}{m^5}]$
M1	6.0	1.05	0.702	15.52
M2	7.5	0.84	1.097	56.18
M3	9.0	0.70	1.580	450.64
M4	10.5	0.60	2.148	718.21
M5	12.0	0.52	2.789	727.85
M6	13.5	0.47	3.479	875.83
M7	15.0	0.42	4.188	857.81

matrix. The main diagonal entries of this matrix (**K** in Eq. 1) were tuned to achieve a reasonable match between the motion amplitudes predicted by the numerical model and motion amplitudes recorded during the experiment for a wave period of 6 s. The regular wave cases that were used for model validation in this paper are shown in Tab. I.

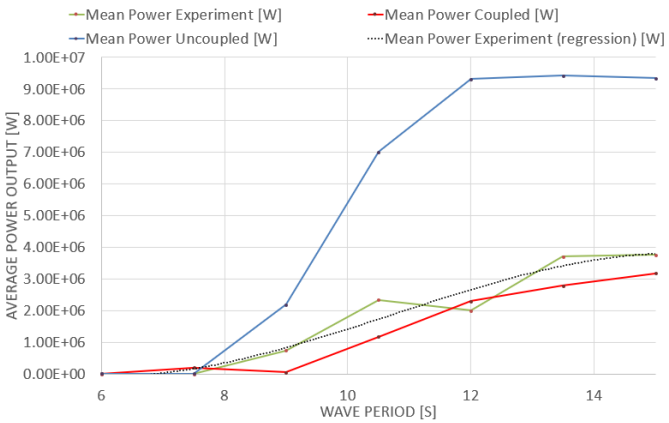

Fig. 12. Average power output from experiment and simulation for different regular waves.

The damping coefficient that is specified to model the pressure drop over the turbine during power extraction is computed from the internal pressure and flow measurements that were collected during the experiment for each of the seven regular wave cases. As outlined in [4], the damping coefficient B_{PTO} in Eq. 2 and Eq. 3 is computed as:

$$B_{PTO} = \frac{\Delta P}{Q} \tag{11}$$

with ΔP being the pressure drop over the turbine and Q being the flow rate through the turbine.

A comparison between the average power recorded during the experiment and the average power from the numerical simulation (coupled/floating and uncoupled/fixed model) is shown in Fig. 12. As expected from the RAO analysis, the coupled system produces more power for smaller wave periods and significantly less power than the uncoupled system for larger wave periods. Experimental power performance data and the simulated power performance of the coupled system are in relatively good agreement.

A comparison between the pitch motion amplitude of the coupled/floating and the uncoupled/fixed numerical model and the pitch motion amplitude recorded during the experiment is shown in Fig. 13.

The pitch resonance peak at about 0.5 rad/s (Fig. 6 is clearly evident for the uncoupled model for wave periods of about 12 s. The overall pitch motion of the uncoupled system appears to be larger than what was recorded during the experiment. Additional tuning of the mooring stiffness matrix could help to improve the match between the simulated and experimental pitch motion amplitude. The larger pitch motion amplitude should also have a negative effect on the power production of the coupled model as discussed in the previous section. Further tuning of the mooring stiffness should therefore also decrease the differences in average power observed between the coupled model and the experimental data, as shown in Fig. 12.

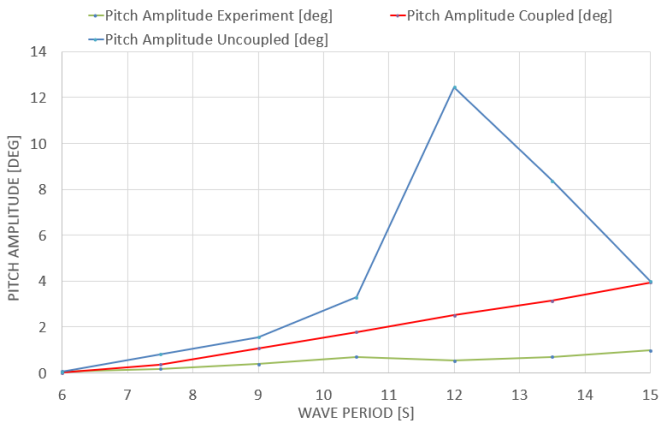

Fig. 13. Pitch motion amplitude from the experiment and simulation for different regular waves.

VI. Conclusion

A scaled version of the M3 device has been tested in a floating/moored configuration at the Marine Hydrodynamics Laboratory (University of Michigan) during the U.S. Department of Energy Wave Energy Prize in 2016. The device motion and power performance were recorded during the test campaign. Based on the equations introduced in [4], the authors developed a numerical model to simulate the M3 device as a floating and a fixed system. To study the power performance of the fixed numerical model, all coupling terms were simply set to zero. Given the larger uncertainty associated with the experimental data, relatively good agreement was found in terms of pitch motion and power performance between the experimental data and the floating/coupled numerical model. Coupling between the pitch and bag motion was found to have positive effects on power production for certain wave frequency regions. The relative phase between pitch motion response and the bag displacement is a key factor regarding the power performance of the floating device.

Acknowledgment

The Alliance for Sustainable Energy, LLC, (Alliance) is the manager and operator of the National Renewable Energy Laboratory (NREL). NREL is a national laboratory of the U.S. Department of Energy, Office of Energy Efficiency and Renewable Energy. This work was authored by the Alliance and supported by the U.S. Department of Energy under Contract No. DE-AC36-08GO28308. Funding was provided by the U.S. Department of Energy Office of Energy Efficiency and Renewable Energy, Water Power Technologies Office. The views expressed in the article do not necessarily represent the views of the U.S. Department of Energy or the U.S. government. The U.S. government retains, and the publisher, by accepting the document for publication, acknowledges that the U.S. government retains a nonexclusive, paid-up, irrevocable, worldwide license to publish or reproduce the published form of this work, or allow others to do so, for U.S. government purposes.

References

[1] K. Gunn and C. Stock-Williams, "Quantifying the global wave power resource," *Renewable Energy*, vol. 44, pp. 296–304, 2012.

[2] A. F. D. O. Falcão, "Wave Energy Utilization: A Review of the Technologies," *Renewable and Sustainable Energy Reviews*, vol. 14, pp. 899–918, 2010.

[3] D. S. Jenne, Y.-H. Yu, and V. Neary, "Levelized Cost of Energy Analysis of Marine and Hydrokinetic Reference Models," in *3rd Marine Energy Technology Symposium*. Washington, DC, United States: METS, 2015.

[4] A. Babarit, F. Wendt, Y.-H. Yu, and J. Weber, "Investigation on the energy absorption performance of a fixed-bottom pressure-differential wave energy converter," *Applied Ocean Research*, vol. 65, pp. 90–101, 2017.

[5] "SBM Offshore." [Online]. Available: https://www.sbmoffshore.com/what-we-do/our-products/renewables/

[6] J. C. McNatt, H. T. Özkan-Haller, M. Morrow, and M. Delos-Reyes, "Preliminary Modeling and Analysis of a Horizontal Pressure Differential Wave Energy Converter," *Journal of Offshore Mechanics and Arctic Engineering*, vol. 136, no. 1, p. 011901, 2013. [Online]. Available: http://offshoremechanics.asmedigitalcollection.asme.org/article.aspx?doi=10.1115/1.4025437

[7] M3 Wave LLC, "M3 wave," https://www.m3wave.com/, 2014.

[8] W. Cummins, "The Impulse Response Function and Ship Motions," David Taylor Model Dasin (DTNSRDC), Tech. Rep., 1962.

[9] F. Wendt, M. Andersen, A. Robertson, and J. Jonkman, "Verification and Validation of the New Dynamic Mooring Modules Available in FAST v8," in *26th International Ocean and Polar Engineering Conference*. Rhodes, Greece: ISOPE, 2016.

[10] F. Wendt, A. Robertson, J. Jonkman, and G. Hayman, "Verification of New Floating Capabilities in FAST v8," in *AIAA SciTech 2015*. Kissimmee, FL: AIAA, 2015.

[11] WAMIT Inc., "Wamit user manual version 7.2," http://www.wamit.com/manualupdate/v72_manual.pdf, 2016.

[12] Z. Steven, "Test Report: Wave Energy Converter Device for M3 Wave Department of Energy Wave Energy Prize 2015," University of Michigan - Marine Hydrodynamics Laboratory - Department of Naval Architecture and Marine Engineering, Michigan, USA, Tech. Rep., 2016.